Mon. Not. R. Astron. Soc. **000**, 000–000 (0000) Printed 26 October 2014 (MN LATEX style file v2.2)

Torus modelling: a code for dynamical modelling of galaxies

Paul J. McMillan, Walter Dehnen, James Binney⋆
Rudolf Peierls Centre for Theoretical Physics, 1 Keble Road, Oxford, OX1 3NP, UK

26 October 2014

ABSTRACT
Torus code is described. Examples are given. It's made publicly available. It's great.

N.B. This is a draft paper. Obviously. It is entirely possible that anything written here is untrue. Including this. I (Paul) have not cleared this text with my co-authors, who should not be blamed for any of its errors.

Key words: Galaxy: fundamental parameters – methods: statistical – Galaxy: kinematics and dynamics

1 INTRODUCTION

Action and angles are the best way of describing orbits. We present a C++ package called DONUT that allows people to work with actions and angles for orbits in axisymmetric potentials on an orbit-by-orbit basis. [1]

The actions $\mathbf{J}$ are constants of motion and are fixed for a given orbit in a given potential Φ. The angles $\boldsymbol{\theta}$ then label a position on the orbit. An orbiting particle in the potential Φ has angles that increase linearly with time, at a rate called the orbital frequency Ω.

Torus modelling was introduced by McGill & Binney (1990) as a method for accessing angle-action coordinates. It was refined by J. (1994).

Torus modelling is incredibly useful, see Binney & McMillan (2011). It has been used to tk tk.

The fundamental operation of torus method, used by DONUT is finding the properties of a given orbit, defined by its three actions $\mathbf{J}$ in a given potential Φ. When this is done, DONUT can find the position and velocity at any point $\boldsymbol{\theta}$ on it.

It is important to note that the torus method is one that finds $\mathbf{x}, \mathbf{v}$ given an input $\mathbf{J}, \boldsymbol{\theta}$, whereas other methods used in the literature (Binney & Spergel 1984; Binney 2012; Sanders & Binney 2014) do the opposite.

2 ANGLE-ACTION COORDINATES

Three actions J_i and three conjugate angles coordinates θ_i provide canonical coordinates for six-dimensional phase space (e.g. Binney & Tremaine 2008, §3.5). The conventional phase space coordinates $\mathbf{w} \equiv (\mathbf{x}, \mathbf{v})$ are 2π-periodic in the angles. The actions are conserved quantities for any orbit, and the angles increase linearly with time:

$$\boldsymbol{\theta}(t) = \boldsymbol{\theta}(0) + \boldsymbol{\Omega}(\mathbf{J})t, \tag{1}$$

where the components of $\boldsymbol{\Omega}$ are the orbital frequencies. Thus, in six-dimensional $(\boldsymbol{\theta}, \mathbf{J})$ space, a bound orbit moves only in the three θ_i directions, over a surface that is topologically a three-dimensional torus. We generally refer to this model of the orbit as "the torus"; it is labelled by the actions $\mathbf{J}$.

Angle-action coordinates exist for any time-independent, integrable Hamiltonian (Arnold 1989). However, an analytic method of computing the transformations between normal phase space coordinates and angle-action coordinates $\mathbf{w} \leftrightarrow (\boldsymbol{\theta}, \mathbf{J})$ is only practical for the Hamiltonian defined by the isochrone potential, which as limiting cases includes the harmonic-oscillator and Kepler potentials (Binney & Tremaine 2008, §3.5.2).

The Hamiltonian corresponding to a more realistic galaxy potential is not necessarily integrable. However usually most orbits in an axisymmetric potential are approximately 'regular' (non-chaotic), and thus admit three approximate isolating integrals of motion, and conjugate angle variables. Consequently, it is possible to find angle-action coordinates which describe motion on these orbits over all interesting time-scales.

tk More detail on this. Including possible perturbation theory.

Methods for constructing angle-action tori for orbits in a general potential have been in the literature for over a decade (McGill & Binney 1990; Kaasalainen & Binney 1994), but have been little utilised, primarily because of the technical challenges these methods present. It is, however, possible to encapsulate these technicalities so that users are protected from them, and once this has been done, it is nearly as easy to construct angle-action coordinates for an

⋆ E-mail: p.mcmillan1@physics.ox.ac.uk

[1] The code is available at the website https://github.com/PaulMcMillan-Astro/Torus

orbit in an axisymmetric potential as it is to numerically integrate the orbit with a Runge-Kutta routine, or similar. This is the intention of DONUT.

3 THE TORUS METHOD

In DONUT we restrict ourselves to orbits in axisymmetric potentials. Conservation of angular momentum about the system's symmetry axis then almost reduces the problem to that of motion in the (R, z) meridional plane in the effective potential

$$\Phi_{\rm eff}(R,z) \equiv \Phi(R,z) + J_\phi^2/2R^2 \tag{2}$$

(e.g. Binney & Tremaine 2008, §3.2) where J_ϕ, the third action, is the conserved component of angular momentum

$$J_\phi = \frac{1}{2\pi}\int_0^{2\pi} p_\phi \,\mathrm{d}\phi = \frac{1}{2\pi}\int_0^{2\pi} L_z \,\mathrm{d}\phi = L_z. \tag{3}$$

The remaining two actions are referred to as J_r and J_z, and, broadly speaking, encode the extent of radial and vertical motion respectively[2]. The conjugate angle coordinates to these actions are $\theta_R, \theta_z, \theta_\phi$, and they increase linearly with time with a frequency that depends on $\Phi_{\rm eff}$ and $\mathbf{J}$

$$\theta_i = \theta_i(t=0) + \Omega_i(\mathbf{J})t. \tag{4}$$

Since the real space coordinates $\mathbf{w} \equiv (\mathbf{x}, \mathbf{v})$ are 2π periodic in the angles, we set each component θ_i to lie in the range $0 \leqslant \theta_i < 2\pi$. We define the zero-point in $\boldsymbol{\theta}$ as the point where an orbit at pericentre and at $z = 0$ with $v_z > 0$ passes Galactocentric $\phi = 0$.

There are some useful rules of thumb for interpreting angle coordinates when this zero-point is defined this way. The value θ_ϕ is approximately the same as the ϕ coordinate of the guiding centre under the epicycle approximation. $\theta_R \sim 0$ corresponds pericentre, $0 <\lesssim \theta_R \lesssim \pi$ to $v_R > 0$ as the orbit goes towards pericentre at $theta_R \sim \pi$, and $\pi <\lesssim \theta_R \lesssim 2\pi$ to $v_R < 0$ as the orbit moves back towards pericentre. Similarly the orbit passes $z = 0$ at $\theta_z \sim 0$, reaches maximum distance above the plane ($z > 0$) at $\theta_z \sim \pi/2$, passes through the plane again (now with $v_z < 0$) at $\theta_z \sim \pi$, then maximum distance below the plane at $\theta_z \sim 3\pi/2$. The approximations for θ_R and θ_z would be exact in the case that motion was separable in R and z. Figure tk shows a typical case.

The torus method is based on a scheme that allows us to go from angle action coordinates to real space coordinates by a step-by-step approach where each step is a canonical transformation and maintains the required properties of the angle action coordinates. Figure 1 shows a schematic diagram illustrating the step-by-step process.

3.1 The generating function

The first step in a torus mapping is to go from the actions and angles in the potential of interest to the actions and angles in a toy potential (one in which the relationship between angle-action coordinates and real-space coordinates is known analytically). This mapping has to ensure that

[2] Note that r and z are simply labels for these actions, and one could equivalently call these J_R and J_ϑ

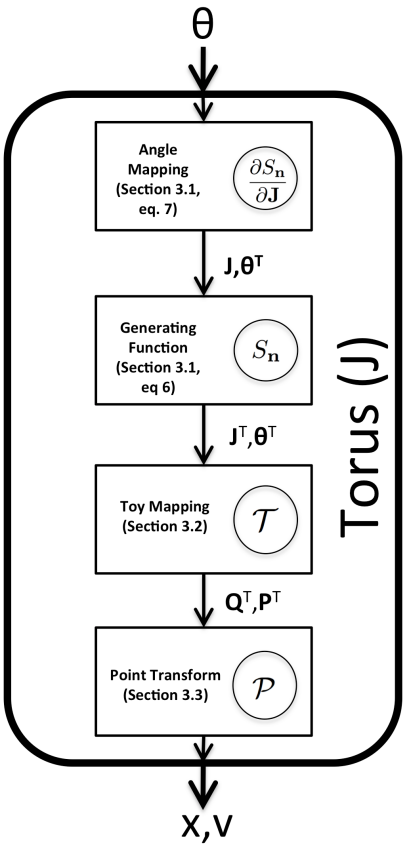

Figure 1. A schematic diagram illustrating the process. The torus with actions $\mathbf{J}$ is defined by the parameters shown in the circles (and explained in later sections), and the positions and velocities $\mathbf{x}, \mathbf{v}$ associated

- The tori remains null in the sense of eq. **??**
- An increase of 2π in any one component of $\boldsymbol{\theta}$ must correspond to an increase of 2π in a corresponding component of $\boldsymbol{\theta}^T$.
- There is enough flexibility to ensure that the torus described is at a constant value of the true Hamiltonian, H – or, to put it another way, that it lies within the hypersurface $H = \text{const}$

The condition that the torus remains null is satisfied by ensuring that the transformation is canonical, which we ensure by using a generating function to define the transformation. Following McGill & Binney (1990) we can use a generating function which is a function of the true actions and the toy angles $S(\mathbf{J}, \boldsymbol{\theta}^T)$ which defines the transformation between $(\mathbf{J}, \boldsymbol{\theta})$ and $(\mathbf{J}^T, \boldsymbol{\theta}^T)$ through the equations

$$J_i = \frac{\partial S(\mathbf{J}, \boldsymbol{\theta}^T)}{\partial \theta_i^T}; \quad \theta_i = \frac{\partial S(\mathbf{J}, \boldsymbol{\theta}^T)}{\partial J_i} \tag{5}$$

The generating function is of the form

$$S(\boldsymbol{\theta}^T, \mathbf{J}) = \boldsymbol{\theta}^T \cdot \mathbf{J} + 2\sum_{\mathbf{n}} S_{\mathbf{n}}(\mathbf{J}) \sin\left(\mathbf{n} \cdot \boldsymbol{\theta}^T\right), \tag{6}$$

where $\mathbf{n}$ is a two-vector with integer components (n_r, n_z), and the values $S_{\mathbf{n}}$ are free parameters.

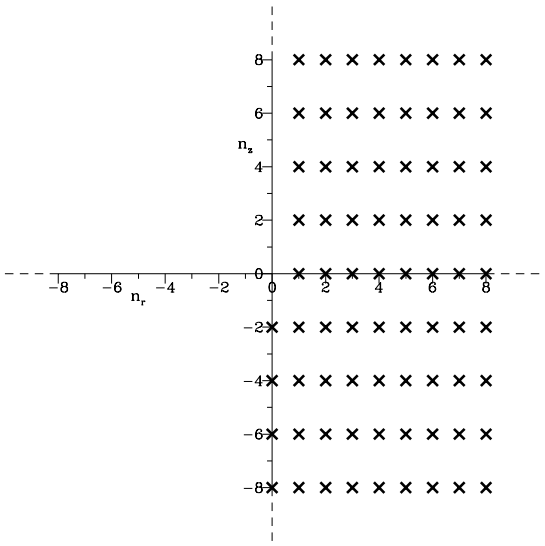

Figure 2. Figure illustrating the pattern of allowed values of (n_r, n_z) in the generating function (eq. 6). Do I seriously need to explain that it doesn't just stop at 8. Isn't that obvious?

This means that at any point $\boldsymbol{\theta}^T$ on the torus with actions $\mathbf{J}$, the toy actions are

$$\mathbf{J}^T = \mathbf{J} + 2\sum_{\mathbf{n}>0} \mathbf{n} S_{\mathbf{n}}(\mathbf{J}) \cos\left(\mathbf{n}\cdot\boldsymbol{\theta}^T\right) \tag{7}$$

(note that, for a given torus, $\mathbf{J}$ is constant, but $\mathbf{J}^T$ varies).

Similarly, the $\boldsymbol{\theta}$ coordinates are given by

$$\boldsymbol{\theta} = \boldsymbol{\theta}^T + 2\sum_{\mathbf{n}>0} \frac{\partial S_{\mathbf{n}}(\mathbf{J})}{\partial \mathbf{J}} \sin\left(\mathbf{n}\cdot\boldsymbol{\theta}^T\right). \tag{8}$$

This form of generating function ensures that the 2π-periodicity of $\boldsymbol{\theta}$ coincides with that of $\boldsymbol{\theta}^T$ and (for convenience) sets $\boldsymbol{\theta} = 0$ where $\boldsymbol{\theta}^T = 0$. The values $S_{\mathbf{n}}$ are all real (this is due to the time-symmetry of the Hamiltonian). The values of n_z are all even, and can be positive or negative (i.e. $n_z = ..., -2, 0, 2, ...$). n_r can take any positive integer value whatever the value of n_z, and can take the value 0 if $n_z < 0$. These restrictions on $\mathbf{n}$ reflect the time symmetry of the Hamiltonian and the reflection symmetry of the potential about $z = 0$. These allowed values are illustrated in Figure 2.

Note that the fitting process (Section 3.4) determines the values $S_{\mathbf{n}}(\mathbf{J})$ at a given $\mathbf{J}$, and then separately determines $\partial S_{\mathbf{n}}(\mathbf{J})/\partial \mathbf{J}$ at that value. It is possible to determine $\partial S_{\mathbf{n}}(\mathbf{J})/\partial \mathbf{J}$ by finite differencing, but it is very succeptable to numerical noise.

3.2 The Toy Mapping

The transformation between toy angle-action coordinates $\mathbf{J}^T, \boldsymbol{\theta}^T$ and some real-space position and momentum coordinates $\mathbf{Q}^T, \mathbf{P}^T$ must be performed using a toy Hamiltonian in which the relationship between the two is known. In the case of DONUT, this is the isochrone potential, which is the most general case where the transformation can be written analytically.

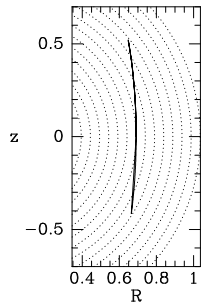

Figure 3. A target shell orbit in the (R, z) plane and circles.

Since one of the actions (J_ϕ) is already known we are able, in the first instance, to work in terms of the reduced 2-dimensional Hamiltonian H^T in a generalised effective isochrone potential

$$\Phi^T_{\rm eff}(r,\vartheta) = \frac{-GM}{b+\sqrt{b^2+(r-r_0)^2}} + \frac{L_z^2}{2\left[(r-r_0)\sin\vartheta\right]^2}, \tag{9}$$

where ϑ is the usual spherical polar coordinate (not to be confused with the dynamical angle coordinates); M, b, L_z and r_0 are free parameters of the toy Hamiltonian. Note that L_z here is a parameter of the toy potential and does not need to be the same as J_ϕ, though it does need to have the same sign. This requirement on the sign of L_z is not because of the motion in the two-dimensional effective potential, which depends on L_z^2 only, but because it ensures that θ^T_ϕ increases in the same sense as θ_ϕ. Appendix A of McGill & Binney (1990) gives the relationships between $J^T_r, J^T_\vartheta, \theta^T_r, \theta^T_\vartheta$ and $r, \vartheta, p_r, p_\vartheta$ in this potential. Expressions for the third angle θ^T_ϕ is given in the appendix of this paper.

The parameters of the effective potential actually used by DONUT are in fact

$$\mathcal{T} = \gamma, \beta, L_z, r_0 \tag{10}$$

γ, β, L_z, r_0 where $\gamma = \sqrt{GM}$ and $\beta = \sqrt{b}$. This means that unphysical negative values of M and b can not be inadvertently chosen during torus fitting.

3.3 Point Transform

N.B. This section doen't make perfect sense. Rewrite will happen.

In an axisymmetric potential the mapping between $\mathbf{J}, \boldsymbol{\theta}$ and $\mathbf{x}, \mathbf{v}$ can be performed for most values of $\mathbf{J}$ using only a generating function and the isochrone potential. However, it is doomed to fail for orbits that have $J_r \ll J_\vartheta$. The values $\mathbf{P}^T, \mathbf{Q}^T$ can simply be transformed into the coordinates system required in the normal way. This can most easily be understood by considering the case as $J_r \to 0$. In this case, eq. 7 will imply negative values of J^T_r unless all of the coefficients $S_{\mathbf{n}}$ also tend to 0, i.e. the transformation must tend towards the identity.

The shell orbits $J^T_r = 0$ of the isochrone potential lie on spheres, but the shell orbits ($J_r = 0$) of a flattened target potential do not (Figure 3). Consequently, along a shell orbit in a flattened potential r oscillates, so $p_r \neq 0$. But if $p_r \neq 0$, then $J^T_r \neq 0$ also, because p_r is non-zero only on an eccentric

orbit. We conclude therefore that a canonical transformation of the form of eq. 7 is insufficiently general to produce image tori that have small radial actions.

The solution to this problem, as described by Kaasalainen & Binney (1994), is to combine the canonical transformation generated by S with a point transformation

$$(r, \vartheta) \rightarrow (r', \vartheta') = (\xi(\vartheta) r, \eta(r)\zeta(\vartheta)) \tag{11}$$

that maps the toy shell orbit into a shell orbit of the target Hamiltonian. Here ξ, η and ζ are functions to be determined. Qualitatively, we want $\eta \sim 1$ and $\zeta \sim \vartheta$; ξ is chosen such that the shell orbit of the target potential is $r' = a$, where a is the radius of the toy shell orbit.

Numerical integration of the target shell orbit yields the radius of this orbit, $r_{\rm s}(\vartheta)$ and we immediately have

$$\xi(\vartheta) \equiv \frac{a}{r_{\rm s}(\vartheta)} \tag{12}$$

because then on the orbit $r' = \xi r_{\rm s} = a$ as required. Figure 4 shows $\xi(\vartheta)$ for the shell orbit plotted in Figure 3.

The generating function of our transformation is

$$S(r, \vartheta, p_r^T, p_\vartheta^T) = \xi r p_r^T + \eta\zeta p_\vartheta^T, \tag{13}$$

so

$$p_r = \xi p_r' + \frac{{\rm d}\eta}{{\rm d}r}\zeta p_\vartheta' \quad ; \quad p_\vartheta = \frac{{\rm d}\xi}{{\rm d}\vartheta} r p_r' + \eta \frac{{\rm d}\zeta}{{\rm d}\vartheta} p_\vartheta'. \tag{14}$$

From our integration of the target shell orbit we know $p_r(\vartheta)$ and $p_\vartheta(\vartheta)$ along this orbit. By construction $p_r^T = 0$ on the target shell orbit, and we choose $p_\vartheta'(\vartheta')$ so it mirrors $p_\vartheta(\vartheta)$ along a shell orbit in the toy potential:

$$p_\vartheta'(\vartheta') = \sqrt{L^2 - \frac{L_z^2}{\cos^2\vartheta'}}. \tag{15}$$

Finally we use the known relation $r_{\rm s}(\vartheta)$ on the target shell orbit to treat η as a function of ϑ. Then equations 14 yield coupled o.d.e.s for η and ζ

$$\frac{{\rm d}\eta}{{\rm d}\vartheta} = \frac{p_r}{\zeta p_\vartheta'} \frac{{\rm d}r_{\rm s}}{{\rm d}\vartheta} \quad ; \quad \frac{{\rm d}\zeta}{{\rm d}\vartheta} = \frac{p_\vartheta}{\eta p_\vartheta'}. \tag{16}$$

Figure 4 shows the functions η and ζ that are obtained by integrating these equations. [3]

So far we have obtained the functions ξ, η and ζ only in the ranges of r and ϑ covered by the closed orbit. The functions are extended beyond this range by adding single points at the ends of the required ranges, and then fitting a sum of Chebychev polynomials to both these points and the points returned by the numerical integrations. The fitting algorithm does not require the polynomial to pass through the given points. Rather a function is constructed from the points by fitting a quadratic to each set of three points. Then the Chebychev series is fitted in a least squares sense to this function – the coefficients of the Chebychev polynomials are found from integrals of the products of the relevant Chebychev polynomial and the quadratics and the weight function. These integrals are done analytically. By relieving the polynomial of the obligation to pass through the data points, this techniques avoids the danger that the polynomial makes wild excursions between data points.

[3] In practice DONUT changes these o.d.e.s to ones with a new independent variable ψ before integrating the equations, where $\vartheta = \vartheta_{\rm max} \sin\psi$, with $\vartheta_{\rm max}$ the largest value of ϑ attained on the closed orbit.

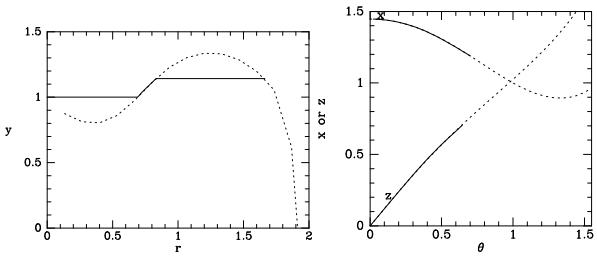

Figure 4. The functions $\eta(r)$ (left) and $\xi(\theta)$, $\zeta(\theta)$ (right) that define the new (r', θ') coordinates. The full curves show results obtained by integrating the defining equations and then adding extra points to fill out the range, while the dashed curves show Chebychev-polynomial L^2 fits to the points defined by these curves.

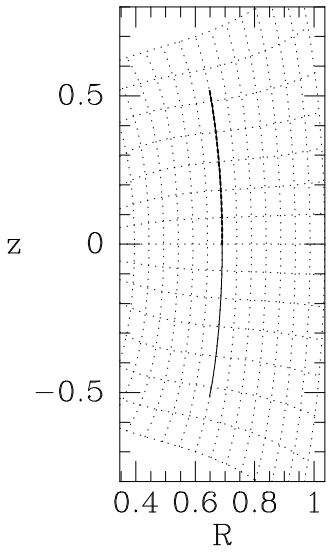

Figure 5. The dotted lines show the (r, ϑ) coordinate system constructed such that a shell orbit in the target potential coincides with a curve of constant r.

Figure 5 shows the new coordinates, while Figure 6 shows the fits obtained to the target shell orbit in the (r, p_r) and (r, p_θ) planes. When a point transformation is used in addition to the canonical transformation generated by equation 6, the scheme is summarised by

$$(\boldsymbol{\theta}, \mathbf{J}') \xrightarrow{\rm S} (\boldsymbol{\theta}, \mathbf{J}) \xrightarrow{\rm isoch} (r, \vartheta, p_r, p_\vartheta) \xrightarrow{H} (\xi(\vartheta) r, \eta(r)\zeta(\vartheta), p_{r'}, p_{\vartheta'}) \,. \tag{17}$$

The parameters of the point transform are the coefficients of the Chebyshev polynomial, and we indicate them with the symbol $\mathcal{P}$.

3.4 Fitting a Torus

A torus is defined by a value $\mathbf{J}$ of the actions. The transformation between $\boldsymbol{\theta}$ and $\mathbf{x}, \mathbf{v}$ is then defined by the parameters of the point transform $\mathcal{P}$ (if needed), the parameters of the toy isochrone potential $\mathcal{T}$, the paramters of the generating function $S_{\mathbf{n}}$ and their partial derivatives with respect to $\mathbf{J}$. This is done in two stages, which we refer to as the "action fit" and the "angle fit".

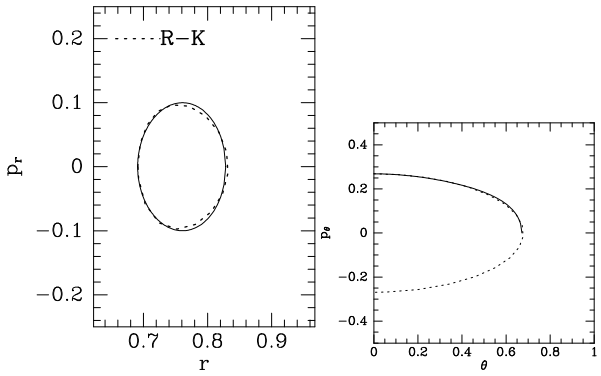

Figure 6. Fits in the two position-momentum planes: dotted curves numerical integration, full curves images of the harmonic oscillator under the point transformation.

3.4.1 Action fit

The values $S_{\mathbf{n}}(\mathbf{J})$ and $\mathcal{T}$ corresponding to a given gravitational potential and $\mathbf{J}$ are found by enforcing the condition that the Hamiltonian H is constant on the target torus. Remarkably this condition is sufficient to ensure that the torus corresponds to an orbit in the given galaxy potential (McGill & Binney 1990).

The practical method by which we attempt to enforce this condition is by finding the value of the Hamiltonian H at $N_{\rm p}$ points spread evenly in $\boldsymbol{\theta}^T$ over the torus for some trial set of parameters, and then seek to minimize the variation over the torus, which we define with the statistic

$$\chi^2 = \frac{1}{N_{\rm p}} \sum (H - \overline{H})^2, \tag{18}$$

where $\overline{H} = \sum H/N_{\rm p}$. We minimize using the Levenberg-Marquardt algorithm (e.g. Press et al. 1986). The derivatives of H with respect to the $S_{\mathbf{n}}$ and the parameters of the toy Hamiltonian that the Levenberg-Marquardt algorithm requires can all be found through the chain rule. The time symmetry and symmetry about $z = 0$ means that we only need to consider points with $0 \leqslant \theta_r < \pi$ and $0 \leqslant \theta_z < \pi$.

The more parameters are being fit simulataneously, the slower the fitting process. This is primarily because the number of derivatives that have to be calculated at each step increases with the number of parameters that are fit. We therefore start by varying only the parameters of the toy potential, fixing all values of $S_{\mathbf{n}} = 0$. We then allow the value $S_{\mathbf{n}}$ to vary (as well as $\mathcal{P}$) for a small number of low order terms.[4] If this provides a torus with a sufficiently small value of χ^2 we stop the action fit at this point. If not, we allow other, higher order, terms to vary as well and repeat the process until a sufficiently small value of χ^2 is achieved, or this process has been repeated a large number of times (we typically set the maximum number of repeats as 10, at which point there are typically ~ 700 values of $S_{\mathbf{n}}$ being used in the series expansion).

When allowing additional terms $S_{\mathbf{n}}$ to vary, we attempt to ensure that the values $\mathbf{n}$ we chose are those which are most important for fitting the orbit. To do that we add new terms adjacent to any term for which $S_{\mathbf{n}}$ has an absolute value above a threshold value.[5] The threshold is set as a fraction of the highest value of $S_{\mathbf{n}}$ for any $\mathbf{n}$.

The criterion we apply to χ^2 to decide whether the action fit is good enough motivated by the idea that what we really care about is how close $\mathbf{J}$ is to the true value at a given $\mathbf{x}, \mathbf{v}$. We recognise that we can relate that to χ^2 via the relationship $\partial H/\partial \mathbf{J} = \boldsymbol{\Omega}$, and require that

$$\chi^2 \leqslant \left(\mathrm{TOL}_J \tilde{\Omega} \tilde{J} \right)^2 \tag{19}$$

where TOL_J is a tolerance parameter,

$$\tilde{\Omega} = \sqrt{\Omega_R^2 + \Omega_z^2} \tag{20}$$

is a scale frequency and

$$\tilde{J} = \begin{cases} \sqrt{J_r \times J_z} & \text{if } J_r \neq 0 \text{ and } J_z \neq 0 \\ J_r + J_z & \text{otherwise.} \end{cases} \tag{21}$$

is a scale action. The value TOL_J can therefore be thought of as an allowed tolerance in the fractional accuracy of $\mathbf{J}$.

The choice of expression for $\tilde{J}$ is a compromise between an expression that takes the scale to be of order the larger or smaller of the two actions. This is necessary because if, say, we have $J_r \gg J_z$ then taking $\tilde{J} \sim J_r$ would mean that the constraint was very weak compared to the total variation in energy that could plausibly be associated with motion in the z-direction, whereas taking $\tilde{J} \sim J_z$ would provide an excessively stringent constraint on accuracy required in describing the radial motion.

The tolerance parameter TOL_J is left as something that the end-user of DONUT can adjust, but with a default value of 0.003. We have found that it is, in general, not a good idea to adjust TOL_J to a significantly lower value. The most obvious reason for this is that satisfying more stringent constraints requires more terms in the generating function, which takes more computing time. A more fundamental reason is that there are some instances, such as near resonances, where there is no torus of the chosen form which corresponds to an orbit in the true Hamiltonian. In these cases attempting to minimize χ^2 beyond a certain point is fruitless at best, and can lead to overfitting.

In some applications, such as stream fitting when one is far from a resonance, it may be appropriate to take a smaller value of TOL_J. In the case of streams this is because one is considering a relatively small volume in phase-space, so a precise determination of the actions is useful. It is likely that this criterion on χ^2 could be improved, perhaps by determining the point at which adding further terms stops producing a significant improvement in the fit, but this is not currently implemented in DONUT.

3.4.2 Action fit with a point transform

The above description of how we find the parameters $S_{\mathbf{n}}$ and $\mathcal{T}$ is suitable for the case where no point transform (Section 3.3) is required. As we have shown, there are some instances, with $J_z \ll J_r$ where this approach will fail. In

[4] In the current implementation these are $(n_r, n_z) = (0,-4),\ (0,-2),\ (1,-2),\ (1,-0),\ (1,2),\ (1,4),\ (2,-2),\ (2,0),\ (3,0)$.

[5] so, for example if $|S_{3,-10}|$ is above the threshold, $S_{2,-10}$, $S_{3,-12}$, $S_{3,-8}$ and $S_{4,-10}$ are added to the values allowed to vary if they were not already allowed to.

these instances we find the appropriate point transform for the torus using the method described in section 3.3 which, by construction, requires that a circular orbit in the toy potential with the same J_z and J_ϕ is at $r = 1$. The parameters of the toy potential $\mathcal{T}$ are therefore strongly constrained, with $r_0 = 0$, $L_z = J_\phi$, and since we have complete freedom to choose β, and some freedom to chose γ, we set $\beta = \sqrt{3}$ and chose γ to ensure that the circular orbit goes through $r = 1$ as required.

When this has been done we fit the values of $S_\mathbf{n}$ as above, except that the parameters of the toy potential are not allowed to vary.

3.4.3 Angle fit

The action fit determines the functional dependence $\mathbf{w}(\boldsymbol{\theta}^T, \mathbf{J})$. It therefore provides enough information to know all of the phase-space points $\mathbf{w}$ that the torus goes through. However, it does not tell us how $\mathbf{w}$ depends on $\boldsymbol{\theta}$: the values $S_\mathbf{n}$ have been determined for a single value of $\mathbf{J}$, so $\partial S_\mathbf{n}(\mathbf{J})/\partial \mathbf{J}$ is still undetermined.

To find the orbital frequencies $\boldsymbol{\Omega}$ and the values $\frac{\partial S_\mathbf{n}(\mathbf{J})}{\partial \mathbf{J}}$ expressions for the angle coordinates, we integrate small sections of the orbit, starting from a grid of points on the torus, and use the equations (Kaasalainen & Binney 1994)

$$\boldsymbol{\theta}(0) + \boldsymbol{\omega} t = \boldsymbol{\theta}^T(t) + 2\sum_{\mathbf{n}>0} \frac{\partial S_\mathbf{n}(\mathbf{J})}{\partial \mathbf{J}} \sin[\mathbf{n}\cdot\boldsymbol{\theta}^T(t)]. \qquad (22)$$

Each integration for M time-steps yields $3M$ such equations in which $\boldsymbol{\theta}(0)$, $\boldsymbol{\omega}$, and $\partial S_\mathbf{n}(\mathbf{J})/\partial \mathbf{J}$ are unknowns. The equations are linear in the unknowns and for $M \gg 1$ the number of available equations increases much faster than the number of unknowns. We truncate the sum over $\mathbf{n}$ to ensure that the number of unknowns is significantly less than the number of equations, and solve the equations using a least squares fit. We refer to this process as an "angle fit".

tk details

4 TECHNICAL DETAILS

In the interests of clarity, and providing an introduction to the code DONUT, we describe here how the basic structure of the code relates to the method described in this paper. The code is written in C++, and is therefore object oriented. In this section we describe the important classes and what they contain.

The class *Potential* is a base class for any axisymmetric potential, each of which must return the potential and its derivatives with respect to R and z at a given point. It also returns epicycle frequencies, and the angular momentum of a circular orbit at a given radius R. of a given J_ϕ (or the value of . The DONUT package includes classes for various different potentials including the class *GalaxyPotential* which gives the potential associated with a given density distribution consisting of exponential discs (with or without central holes) and spheroids, using the method described by Dehnen & Binney (1998).

The complete working of the code is encapsulated in the class *Torus*. It has a member function *AutoFit* which, given a *Potential* and a value of the actions, finds the corresponding torus using the method described in Section 3.4. Once this has been done there is a member function of *Torus* that can find the values of $\mathbf{x}$ and $\mathbf{v}$ corresponding to a given value of $\boldsymbol{\theta}$. There are also member functions that can determine whether a torus goes through a given point $\mathbf{x}$, and if so with what velocities – there are 4 possible velocities at any position that the torus passes – and what the density of the torus is at that point. If the torus does not pass through that position, there is a member function that determines how close to that point it gets.

The various steps shown in Figure 1 each have their own associated class (that is also a member of *Torus*).

The class *AngMap* handles the mapping between $\mathbf{J}, \boldsymbol{\theta}$ and $\mathbf{J}, vtheta^T$ (eq. 8). This mapping works in either direction, and the values $\partial\theta_i/\partial\theta_j^T$ can also be found. The parameters are a set of values of $\mathbf{n}$ and corresponding values $\partial S_\mathbf{n}/\partial J_R$, $\partial S_\mathbf{n}/\partial J_z$ and $\partial S_\mathbf{n}/\partial J_\phi$. These are stored in the class *AngPar*, which is a member of *AngMap*.

The class *GenFnc* handles the mapping from $\mathbf{J}, \boldsymbol{\theta}^T$ to $\mathbf{J}^T, \boldsymbol{\theta}^T$ (eq. 7). Note that this only works in the direction of finding $\mathbf{J}^T$ at a given $\boldsymbol{\theta}^T$ for the fixed value of $\mathbf{J}$. It also finds the derivatives $\partial\mathbf{J}^T/\partial\boldsymbol{\theta}^T$. The parameters, $\mathbf{n}$ and corresponding $\S_\mathbf{n}$, are stored and manipulated by the class *GenPar*.

The class *GenFncFit* performs the same tasks as *GenFnc* but focusses on the transformations required when performing an action fit (Section 3.4.1), where we have a known, regular grid of points in $\boldsymbol{\theta}^T$ where the transformation has to be calculated many times. It also provides the derivatives $\partial\mathbf{J}^T/\partial S_\mathbf{n}$.

The class *ToyMap* is a base class for any mapping between $\mathbf{J}^T, \boldsymbol{\theta}^T$ and $\mathbf{P}^T, \mathbf{Q}^T$. The only class of this kind that is implimented is *ToyIsochrone* which gives the mapping in the generalised effective isochrone potential (Section 3.2). It can also calculate the partial derivatives of $\mathbf{P}^T, \mathbf{Q}^T$ with respect to $\mathbf{J}^T$, $\boldsymbol{\theta}^T$ or the paramters of the toy potential.

The class *PointTransform* is a base class for any point transform to convert from $\mathbf{P}^T, \mathbf{Q}^T$ to the output coordinates. If no point transform is required this is done by the class *PointNone*. If one is required because the orbit is close to a shell orbit, a point transform of the kind described in Section 3.3 is implemented by the class *PoiClosedOrbit*.

5 EXAMPLES

In all cases we work in the 'best' Milky Way potential found by McMillan (2011), which is produced by a mass distribution consisting of two exponential discs (representing the thin and thick stellar discs), an axisymmetric bulge and a spherically symmetric dark matter halo.

5.1 Basic example

As a first (trivial) example we demonstrate that the torus fitting does produce accurate descriptions of orbits in typical Galactic potentials. In Figure 7 we show plots demonstrating this for four orbital tori. We choose one torus with $J_r, J_z \ll J_\phi$ (a small deviation from a circular orbit); one with $J_r \ll J_z$ (close to the closed shell orbit); one with $J_r \gg J_z$ (a nearly planar orbit); and one with $J_r \sim J_z \sim J_\phi$ (a halo-like orbit). In each case we set the tolerance threshold $\text{TOL}_J = 0.0002$.

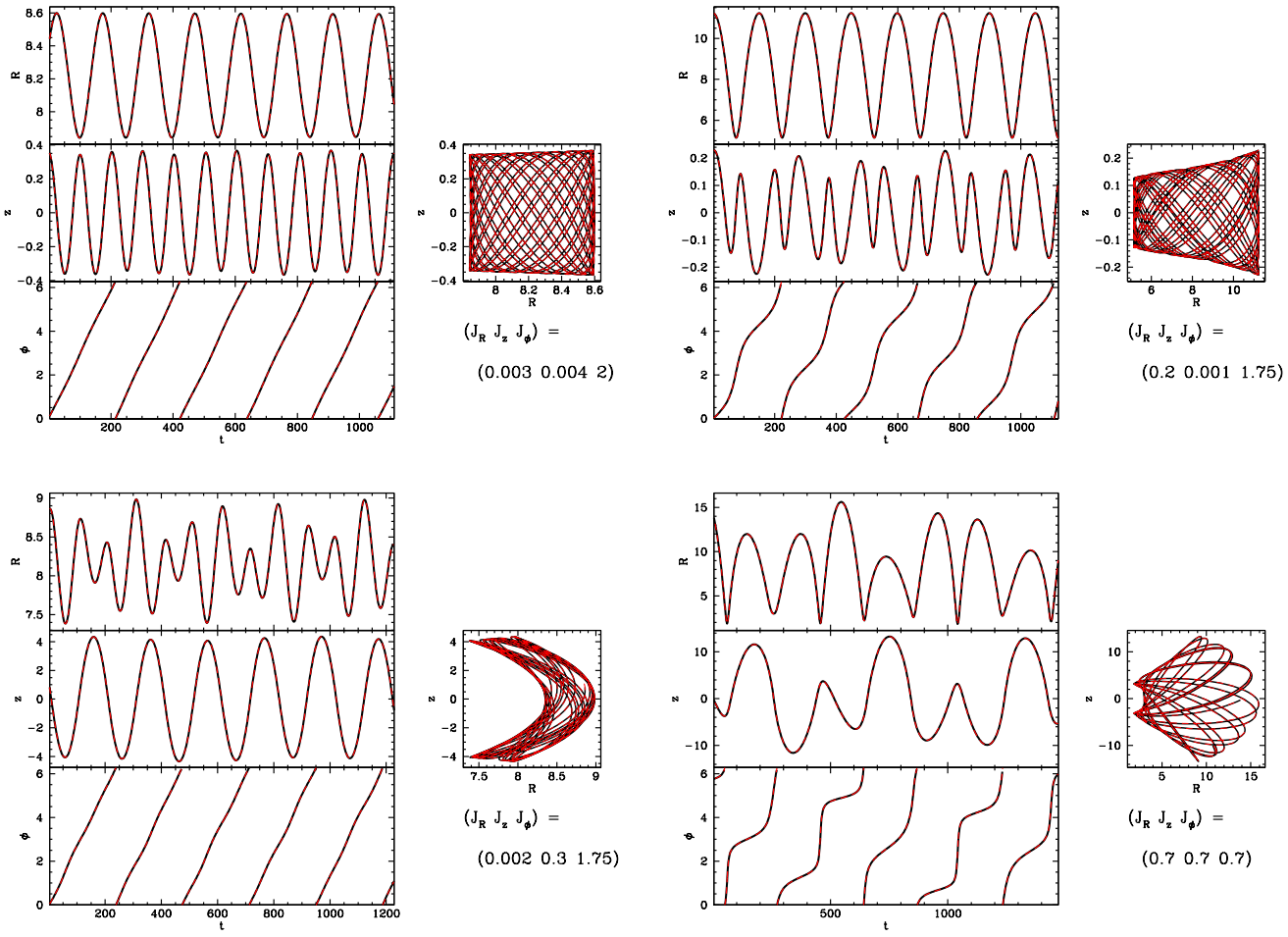

Figure 7. Orbits found by tracing the path associated with the expected linear increase in $\boldsymbol{\theta}$ using the torus machinery (solid black lines) or by Runge-Kutta integration in the gravitational potential (red dashed lines). The two agree to high precision.

For each torus we chose a starting point $\boldsymbol{\theta}$ at random, convert it to a phase space position $\mathbf{x}, \mathbf{v}$ using the torus machinery then follow the orbit by two methods

- Integrating the orbit path in the potential in the real phase space using a Runge-Kutta integrator (i.e. without using the torus machinery).
- Following the linear increase in $\boldsymbol{\theta}$ with known frequency $\boldsymbol{\omega}$ (eq. 1), and converting this angle to $\mathbf{x}, \mathbf{v}$ using the torus machinery.

As Figure 7 shows, the torus machinery very accurately reproduces the integrated orbit in all these cases.

The value of TOL_J used for these examples significantly lower than we typically use for most modelling – this demonstrates the accuracy with which torus modelling can reproduce orbits that are far from resonance. However in the general case we have to consider the problems that can arise when we are near resonance, which is why we usually take a larger value for TOL_J (as discussed in Section 3.4.1.

In Figure 8 we show an example of an orbit trapped at resonance, and a fitted torus that intersects it in phase space. In this case we set $\mathrm{TOL}_J = 0.003$. The torus provides a good fit to the motion in the $R-z$-plane over the timescale of the integration used to create the figure. However, the surface of section shows that the two will inevitably diverge over a longer timescale, because the integrated orbit will remained trapped around the resonance, while following the torus model it will explore other regions of phase-space.

tk explain more.

5.2 Equilibrium distribution

Sample from $f(J)$, show that its in equilibrium in the underlying potential.

5.3 Stream

A great deal of work in recent years has gone into describing stream formation in terms of action-angle coordinates (e.g. Helmi & White 1999, Eyre & Binney 2011, Sanders passim, Bovy 2014, Fardal et al 2014). Using DONUT it is straightforward to generate realisations of streams given a model distribution in action-angle space.

Quick explanation of the idea.

Consider a progenitor with a velocity dispersion σ_v and scale radius r_s. Following Eyre & Binney 2011 and Bovy

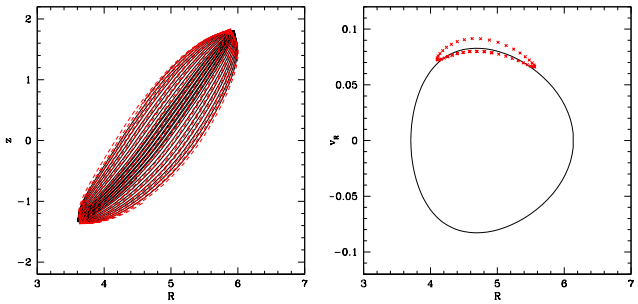

Figure 8. Orbit shown in the $R-z$-plane (left) and as a surface of section (i.e. values of R and v_R as the orbit passes $z = 0$ with $v_z > 0$). The black line is found by tracing the path associated with the expected linear increase in $\boldsymbol{\theta}$ using the torus machinery.The red dashed line and croses by Runge-Kutta integration in the gravitational potential. The surface of section shows that the true orbit is trapped at resonance.

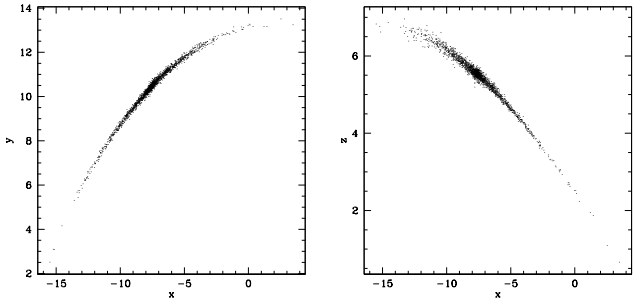

Figure 9. Stars sampled from the action-angle model of a stream. The figures show the positions of particles in the $x-y$ and $x-z$ planes. Look at it. All streamy. Mmmm.

2014 we can write down approximations for the associated dispersion in the three actions

$$\sigma_{J_r} \approx \frac{1}{\pi}\sigma_v\,(r_{\rm apo} - r_{\rm peri}), \tag{23}$$

$$\sigma_{J_z} \approx \frac{2}{\pi}\sigma_v Z_{\rm max}, \tag{24}$$

$$\sigma_{J_\phi} \approx \sigma_v\, r_{\rm peri}, \tag{25}$$

where tk explain symbols. Further we note that we can find approximate values for the dispersion in $\boldsymbol{\theta}$

$$\sigma_{\theta_r} \approx \pi\frac{r_{\rm s}}{(r_{\rm apo} - r_{\rm peri})}, \tag{26}$$

$$\sigma_{\theta_z} \approx \pi\frac{r_{\rm s}}{2\,Z_{\rm max}}, \tag{27}$$

$$\sigma_{\theta_\phi} \approx \frac{r_{\rm s}}{r_{\rm peri}}, \tag{28}$$

We therefore have tk describe model - $\mathbf{J}$ chosen from multivariate Gaussian about action of progenitor, $\boldsymbol{\theta}$ chose from one around $\boldsymbol{\theta}$ progenitor plus $(\boldsymbol{\Omega}(\mathbf{J}) - \boldsymbol{\Omega}(\mathbf{J}_{rmprog}))\,t$ where t is sampled from a uniform distribution between 0 and $t_{\rm max}$.

N.B. this 'stream' model includes stars in the progenitor. Improvement needed.

An example is shown in Figure 9 where we have used DONUT to populate a model of the kind described for a disrupted cluster with $\sigma_v = 2\,{\rm km\,s^{-1}}$ and $r_s = 0.05\,{\rm kpc}$, with $t_{\rm max} = 2\,{\rm Gyr}$.

5.4 Disc substructure

Make a moving group like the Hyades.

6 DISCUSSION AND CONCLUSIONS

You know, I've learned something today...

REFERENCES

Arnold V., 1989, Mathematical methods of classical mechanics, Vol. 60. Springer
Binney J., 2012, MNRAS, 426, 1324
Binney J., McMillan P., 2011, MNRAS, 413, 1889
Binney J., Spergel D., 1984, MNRAS, 206, 159
Binney J., Tremaine S., 2008, Galactic Dynamics: Second Edition. Princeton University Press
Dehnen W., Binney J., 1998, MNRAS, 294, 429
J. K. M. K., 1994, Ph.D. Thesis
Kaasalainen M., Binney J., 1994, MNRAS, 268, 1033
McGill C., Binney J., 1990, MNRAS, 244, 634
McMillan P. J., 2011, MNRAS, 414, 2446
Press W. H., Flannery B. P., Teukolsky S. A., 1986, Numerical recipes. The art of scientific computing. Cambridge: University Press, 1986
Sanders J. L., Binney J., 2014, MNRAS, 441, 3284

APPENDIX A: EVALUATING θ_ϕ^T IN THE ISOCHRONE POTENTIAL

Evaluating θ_ϕ^T in the generalised effective isochrone potential potential (eq. 9) is not, perhaps, as straightforward as might appear from the standard texts. We therefore give the details here.

First let us consider the usual case where $J_\vartheta \neq 0$ (with ϑ the usual polar angle). We have found the values of $\theta_r^T, \theta_\vartheta^T$ and $\boldsymbol{J}$ (or equivalently $r, \vartheta, p_r, p_\vartheta$) in the generalised effective isochrone potential potential (eq. 9). For the standard isochrone potential ($r_0 = 0$, no term in L_z), we have from equations (3.229) and (3.232) of Binney & Tremaine (2008) that

$$\theta_\phi = \phi - u + {\rm sgn}(L_z)\theta_\vartheta \tag{A1}$$

with ϕ the usual azimuthal angle and

$$\sin u \equiv \cot i \cot\vartheta, \tag{A2}$$

with i the inclination given by $i = \arccos(L_z/L)$.

Care needs to be taken when finding i and u. i is found in the toy Hamiltonian, so L_z is the value used as a parameter in eq.9, and $L = J_\vartheta^T + |L_z|$.

Equation A2 only provides the value of $\sin u$, while u takes values throughout the range $(0, 2\pi)$, so this is insufficient. We need to take note of the fact that $u = \phi - \Omega$, where in this case Ω is the longitude of the ascending node, the line on which an orbit crosses the $x-y$ plane with $\dot\vartheta < 0$, (again, in the spherical toy potential, in which the orbital

plane does not precess). Assume that $L_z > 0$ and follow the star up from the ascending node (where $u = 0$) until ϑ stops decreasing. Then it is geometrically clear that $\vartheta = \pi/2 - i$, so $\sin u = 1$ and $u = \pi/2$. Now ϑ starts to increase and in order to ensure that u continues to increase we need to shift to the other solution of eq. A2, $u = \pi - \arcsin(\cot i \cot \vartheta)$.

In summary for $L_z > 0$ we take

$$u = \begin{cases} \arcsin(\cot i \cot \vartheta) & \text{for} \dot{\vartheta} < 0 \\ \pi - \arcsin(\cot i \cot \vartheta) & \text{otherwise.} \end{cases} \quad \text{(A3)}$$

With this definition, $-\pi/2 < u < 3\pi/2$.

When $L_z < 0$, $i > \pi/2$ and u decreases from zero as the star rises through the ascending node, just as ϕ decreases, and eq A2 still applies.

A1 Planar orbits

When $J_\vartheta = 0$, the value of θ_ϑ is undefined, so eq. A3 is essentially meaningless. We have to return to the full expression for the generating function, equation 3.231 of Binney & Tremaine (2008), fixing $J_2 = |J_1| \equiv |L_z|$, and $\vartheta = \pi/2$:

$$S = \phi L_z + \int_{r_{min}}^{r} \mathrm{d}r\, \epsilon_r \sqrt{2H(L_z, J_r) - 2\Phi(r) - \frac{L_z^2}{r^2}}, \quad \text{(A4)}$$

and find $\theta_\phi = \partial S/\partial L_z$. Happily, this is very similar to the equations that have already been solved to find θ_ϑ in the usual case, so we know that we can solve for θ_ϕ:

$$\theta_\phi = \phi + \frac{\Omega_\phi}{\Omega_r}\theta_r - \mathrm{sgn}(L_z) \left[\tan^{-1}\left(\sqrt{\frac{1+e}{1-e}} \tan\left(\frac{1}{2}\eta\right) \right) + \frac{1}{\sqrt{1+4GMb/L_z^2}} \tan^{-1}\left(\sqrt{\frac{1+e+2b/c}{1-e+2b/c}} \tan\left(\frac{1}{2}\eta\right) \right) \right], \quad \text{(A5)}$$

where e, η and c are as defined in eq. 3.240 of Binney & Tremaine (2008).